Methanol synthesis through sorption enhanced carbon dioxide hydrogenation

Maksimov Pavel, Laari Arto, Ruuskanen Vesa, Koiranen Tuomas, Ahola Jero

DOI: 10.1016/j.cej.2021.129290

Full title of the paper:

Methanol synthesis through sorption enhanced carbon dioxide hydrogenation

Authors:

Pavel Maksimov[(a)*], Arto Laari[(a)], Vesa Ruuskanen[(b)], Tuomas Koiranen[(a)], Jero Ahola[(b)]

Authors' affiliations:

[(a)] Lappeenranta-Lahti University of Technology, LUT School of Engineering Science, Yliopistonkatu 34, 53850 Lappeenranta, Finland. P.O. Box 20, FI-53851 Lappeenranta, Finland.

[(b)] Lappeenranta-Lahti University of Technology, LUT School of Energy Systems, Yliopistonkatu 34, 53850 Lappeenranta, Finland. P.O. Box 20, FI-53851 Lappeenranta, Finland.

[*] Corresponding author: E-mail: pavel.maksimov@lut.fi (P. Maksimov)

Corresponding author at: Lappeenranta-Lahti University of Technology, LUT School of Engineering Science, Yliopistonkatu 34, 53850 Lappeenranta, Finland. P.O. Box 20, FI-53851 Lappeenranta, Finland.

Abstract

Synthesis of methanol from carbon dioxide is affected by thermodynamic limitations and excessive formation of water that might have a detrimental impact on methanol production rate and catalytic activity. To overcome these effects, sorption enhanced (SE) carbon dioxide hydrogenation to methanol with selective in-situ adsorption of water is investigated both experimentally and via process simulation. A significant improvement in the process performance due to the thermodynamic equilibrium shift, achieved as a result of selective water removal, is reported. Depending on the process conditions, during the SE phase, outlet methanol concentration is ca. 150-290 % of the steady state values recorded after the adsorbent saturation. For carbon monoxide this factor is ca. 220-510 %. The effect of process parameters such as reactor pressure, temperature, overall gas flowrate and catalyst-to-adsorbent ratio is thoroughly addressed. Reactor pressure is demonstrated to affect methanol production during the SE phase to the greatest extent. Particularly, increasing reactor pressure above 40 bar enhances methanol formation during the SE phase at the cost of decreasing carbon monoxide production, thus improving process selectivity. Although increasing reactor temperature above 250 ^{o}C favors carbon monoxide formation, it results in suppressed methanol production and considerable shortening of the SE phase duration. Because of the RWGS reaction fast kinetics, the variations in gas hourly space velocity and amount of the adsorbent loaded in the reactor affect production of methanol more than carbon monoxide. The parameters describing kinetics of the involved reactions and water adsorption are adjusted based on the acquired experimental data.

Keywords

Sorption enhancement; Methanol synthesis; CO_2 hydrogenation; Dynamic modeling

Highlights

- 3Å molecular sieve is mixed with methanol synthesis catalyst to adsorb water
- Significant temporary improvement in efficiency is achieved due to water removal
- The process is studied for a wide range of industrially relevant conditions
- Mechanistic process model is developed for investigating temporal process changes
- Downstream processing can be simplified as methanol is the only liquid product

Notation

Greek symbols

ε_b	bed porosity (considers the void volume in the bed);
ε_p	particle porosity (considers the void volume inside a particle);
ε_t	total bed porosity (considers the total void volume $\varepsilon_t = \varepsilon_b + (1 - \varepsilon_b)\,\varepsilon_p$);
$\rho_{ads,p}$	adsorbent particle density, kg/m^3;
ρ_{ads}	adsorbent bulk density, kg/m^3;
ρ_{cat}	catalyst bulk density, kg/m^3;
ρ_w	reactor wall density, kg/m^3;
$\vartheta_{i,j}$	stoichiometric coefficient of component *i* for reaction *j*;
μ	gas dynamic viscosity, Pa s;
η_j	effectiveness factor of reaction *j*;

Other symbols

A_i	pre-exponential factor for adsorption constant of component *i*, mol/(s kg_{cat} bar);
A_j	pre-exponential factor for kinetic rate constant of reaction *j*, mol/(s kg_{cat} bar);
$b_{H_2O,0}$	Langmuir adsorption isotherm fitting parameter, Pa^{-1};
b_{H_2O}	Langmuir adsorption isotherm parameter, Pa^{-1};
$C_{p,a}$	adsorbate heat capacity, J/(mol K);
$C_{p,ads}$	adsorbent heat capacity, J/(kg K);
$C_{p,cat}$	catalyst heat capacity, J/(kg K);
$C_{p,g}$	gas heat capacity, J/(mol K);
$C_{p,w}$	reactor wall material heat capacity, J/(kg K);
D_c	micropore diffusivity, m^2/s;
D_l	axial dispersion coefficient, m^2/sec;
D_p	macropore diffusivity, m^2/s;

$E_{a,j}$ activation energy of reaction *j*, J/(mol);

f_i partial fugacity of component *i*, bar;

h_{in} reactor wall - catalyst/adsorbent mixture heat transfer coefficient, J/(m^2 K sec);

h_{out} reactor wall - reactor wall surroundings heat transfer coefficient, J/(m^2 K sec);

K_i adsorption constant of component *i*, bar^{-1};

$K_{p,j}$ equilibrium constant of reaction *j*;

$k_{(T_{ref})}$ rate constant at reference temperature, mol/(s bar kg$_{cat}$);

k_{LDF} mass transfer coefficient for water adsorption on the adsorbent, s^{-1};

k_f film mass-transfer coefficient for water adsorption on the adsorbent, s^{-1};

k_j kinetic constant of reaction *j*, mol/(s bar kg$_{cat}$);

k_w reactor wall axial thermal effective conductivity, J/(kg K sec);

k_z bed axial effective thermal conductivity, J/(kg K sec);

m_{H_2O} adsorbent saturation capacity, mol/kg;

p reactor pressure, Pa;

q_{H_2O} adsorbent loading, mol/kg;

$q^*_{H_2O}$ equilibrium adsorbent loading, mol/kg;

R universal gas constant, J/(mol K);

R_j rate of reaction *j* per weight of catalyst, mol/(s kg$_{cat}$) ;

r_c micropore radius, m;

r_{in} inner radius of the reactor tube, m;

r_{out} outer radius of the reactor tube, m;

r_p average particle radius, m;

T_{ref} reference temperature, K;

T_{out} reactor wall surroundings temperature, K;

T_w reactor wall temperature, K;

T bed temperature, K;

v interstitial gas velocity, m/s;

y_i component molar fraction;

z	reactor length, m;
$\Delta H_{ads,H_2O}$	heat of water adsorption on the adsorbent, J/(mol);
$\Delta H_{ads,i}^{cat}$	heat of adsorption of component *i* on the catalyst surface, J/(mol);
$\Delta H_{R,j}$	heat of reaction *j*, J/(mol);

Superscripts and subscripts:

i	denotes component;
j	denotes reaction;
e	denotes experiment;
t	denotes a time point during a sorption enhanced synthesis run, min;
ˆ	denotes a component's concentration value obtained from the reactor simulation

List of Acronyms:

WGS	Water Gas Shift;
SE	Sorption-Enhanced;
GHSV	Gas Hourly Space Velocity;
RWGS	Reversed Water Gas Shift;
LDF	Linear Driving Force;
PDEs	Partial Differential Equations;
ODEs	Ordinary Differential Equations;

1. Introduction

In light of the incessant increase in the rate of global greenhouse gas emissions, the necessity of transition towards renewable energy based economy becomes evident. However, intermittent nature of renewable energy sources imposes significant limitations on existing power systems and necessitates development of clean and efficient energy storage technologies [1]. Production of chemical compounds with high energy value using renewable electricity enables efficient energy storage in a conveniently transportable form [2]. Carbon dioxide hydrogenation technologies open up the possibility to utilize H_2 as the main energy carrier and CO_2 as the carbon source. Such an opportunity forms the basis for overcoming the renewable energy storage challenges and reducing net CO_2 emissions at the same time [3]. Methanol is one example of a chemical energy carrier that can be produced by catalytic reduction of CO_2. Aside from being a clean-burning fuel, methanol also finds extensive application as a precursor in chemical synthesis, including production of olefins, formaldehyde, methyl-tert-butyl ether, formic acid, dimethyl ether, acetic acid, biodiesel, and synthetic fuels [4,5]. The volumetric energy density of methanol is, although lower than hydrocarbon fuels, reasonably high, and surpasses even liquid H_2 [6]. Combined with its physical properties, it also makes methanol an efficient energy carrier. Moreover, CO_2-based methanol is estimated to play a crucial role in decoupling the chemical industry from fossil resources in the not so distant future [7].

Traditionally, methanol is produced via gas-phase catalytic conversion of syngas at 50-100 bar pressure and 200-250 ^oC temperature over Cu/ZnO based catalysts [8]. The reactions involved in methanol synthesis can be summarized as follows:

$$CO + 2H_2 \rightleftharpoons CH_3OH \quad \Delta H^0 = -91.0\ \mathrm{kJ/mol} \tag{1}$$

$$CO_2 + H_2 \rightleftharpoons CO + H_2O \quad \Delta H^0 = 41.2\ \mathrm{kJ/mol} \tag{2}$$

$$CO_2 + 3H_2 \rightleftharpoons CH_3OH + H_2O \quad \Delta H^0 = -49.8\ \mathrm{kJ/mol} \tag{3}$$

Importance of methanol synthesis via catalytic reduction of pure CO_2 with renewable H_2 has been widely recognized in the recent years in view of the significant CO_2 utilization potential of the technology [9]. However, methanol synthesis by hydrogenation of pure CO_2 is complicated due to severe equilibrium limitations, which result in low single-pass conversion and, consequentially, increased amount of unconverted reactants in the product stream [10]. This, in turn, necessitates recirculation of the unreacted gases, thereby increasing size and utility consumption of the downstream equipment. An additional issue resides in the increased water formation during direct hydrogenation of pure CO_2. During conventional methanol synthesis from syngas, CO acts as a scavenger of oxygen atoms thus forming CO_2 via the water-gas-shift (WGS) reaction. This way, without CO in the feed stream, water formation is drastically increased [11–14]. Higher water content not only results in a shift of the equilibrium towards the reactants, but also has a detrimental impact on the catalyst [15]. In terms of methanol synthesis catalytic materials, the adverse effect of water mainly involves inhibition of active catalyst sites [16,17] and promotion of catalyst sintering [18,19]. Moreover, some evidence of Cu/ZnO synergy disruption as a result of ZnO crystallization due to presence of water has been reported and linked to permanent reduction of specific catalytic activity [20].

Selective removal of the reaction products with the purpose of shifting the chemical equilibrium towards higher conversions has been recognized as a viable concept for intensification of methanol synthesis process [21]. In one of the pioneering studies on the topic, Westerterp et al. [10] employed a series of two packed tubular reactors with an interstage methanol absorption in between to experimentally verify that a significant increase in single-pass conversion can be achieved by selective product removal. Furthermore, the concept of selective membrane separation of the synthesis products inside the reactor has elicited extensive research interest on the topic of membrane reactors [22]. In the context of methanol synthesis, Struis et al. were the first to suggest and thoroughly investigate the applicability of membrane reactors for methanol synthesis process intensification [23,24]. Through experiments and mathematical modeling of the process, their

studies verified that in-situ removal of the reaction products results in increased methanol production rates. The selective products removal is achieved due to preferential permeation of water and methanol through the membrane. In a similar manner, Chen and Yuan also reported a considerable increase in conversion during methanol synthesis in a membrane reactor [25]. The experimental investigation was, however, limited to rather mild pressure and temperature conditions. Furthermore, some studies were also focused on circumventing the thermodynamic limitations of the process by selectively removing the products from the reaction zone via in-situ condensation [26,27]. The obtained results indicate a significant improvement in conversion of the initial reactants, though at the cost of substantial increase in energy consumption. A novel methanol synthesis reactor concept involving removal of methanol and water from the reaction zone via in-situ absorption by ionic liquids has also been proposed [28].

In terms of the tradeoff between increased energy consumption and improved process performance, the sorption-enhanced (SE) reaction technology is one of the most viable solutions for process intensification via selective removal of reaction products. It involves simultaneous reaction and separation of the products in a single packed bed column filled with an admixture of catalyst and selective sorbent [29]. The concept of sorption enhancement has been successfully applied for intensification of a number of important reactions including CO_2 methanation [30], steam methane reforming [31–34], water gas shift reaction [35–37] and dimethyl ether synthesis [38–40]. Although the SE process provides an opportunity to significantly intensify the equilibrium-controlled reactions, the process is highly transient in nature due to limited sorption capacity. Therefore, to maintain improved process performance an additional sorbent regeneration step should be considered. At the same time, by choosing a selective sorbent with the right affinity the SE process can be designed to produce a pure product.

Although several studies investigated SE methanol synthesis process by modeling and optimization [41–44], experimental verification has been so far rather limited. The gas phase SE methanol synthesis was first experimentally investigated by Terreni et al [45]. More specifically,

a copper-based catalyst supported on commercial 13X zeolite beads was prepared and used for methanol synthesis. A significant temporary increase in production of methanol and CO due to water adsorption onto the zeolite part of the catalyst was demonstrated. The enhancement factor was much more significant for CO than for methanol. Dimethyl ether was also detected in the product stream. However, the process was studied under relatively low pressure of 15 bar, which is not typical for industrial methanol synthesis conditions. Considering that CO_2 hydrogenation reaction (Eq. 3) involves a significant decrease in the total number of moles, the effect of pressure on the performance of SE methanol synthesis is of great interest. Application of a selective adsorbent with a smaller pore diameter and higher saturation capacity is also more beneficial in terms of improved methanol production.

In-situ water adsorption during alcohol-promoted liquid phase methanol synthesis with 3Å molecular sieve was investigated by Nieminen et al. [46], and was also proven to significantly improve the process efficiency. Considering that among the species involved in conventional gas phase methanol synthesis only H_2 and water molecules have effective diameters smaller than 3Å [47,48], it can be speculated that 3Å molecular sieve is a suitable material for selective in-situ water adsorption during gas phase synthesis. In addition to its high selectivity towards water adsorption due to its limited pore diameter, 3Å molecular sieves also possess significant sorption capacity at elevated temperatures, which was demonstrated by van Kampen et al. [49] Moreover, adequate thermal stability under the methanol synthesis conditions and ease of regeneration [50] also make 3Å molecular sieves a particularly suitable material for steam separation in the SE process.

In the current work, SE methanol synthesis via CO_2 hydrogenation is studied over a wide range of industrially relevant conditions with 3Å molecular sieves used as selective water adsorbent. The effect of parameters such as pressure, temperature, catalyst-to-adsorbent ratio, and gas hourly space velocity (GHSV) is investigated in terms of methanol and CO production. For better

understanding of the process, a reactor model is developed and the main parameters characterizing reaction and adsorption kinetics are estimated from the acquired experimental data.

2. Materials and Methods

2.1. Materials

A commercial copper-based methanol synthesis catalyst ($Cu/ZnO/Al_2O_3$, Alfa Aesar) was used in this study. The pelletized catalyst was ground and sieved to obtain a powdered sample with 125-250 μm particle size. 3Å molecular sieve (Alfa Aesar) was used as a water adsorbent for the SE methanol synthesis experiments. The adsorbent was also ground and sieved to produce a 125-250 μm sample. A catalyst/adsorbent mixture was prepared by means of granule mixing at the required mass ratio of the two components as described in [51] and loaded in the reactor.

2.2. Experimental setup and data acquisition

The SE methanol synthesis experiments were conducted in a stainless-steel tubular reactor. While all the details of the experimental setup were reported previously [52], a brief description is provided here as well for the sake of consistency. The core unit of the system is a steel tubular reactor heated with an external electric furnace. Inner diameter of the reactor is 10 mm, while the catalyst/adsorbent mixture bed length is 150 mm. The reactor wall thickness is 1 mm. The reactor temperature is measured and controlled by three K-type thermocouples installed in direct contact with its wall outer surface. The reactor pressure is maintained with a back-pressure regulator. The reactor outlet pipe is connected to a Raman cell equipped with a gas-phase Raman probe (AirHead, Kaiser Optical System, Inc.). The probe serves as an intermediate device transferring the signal to the Raman spectrometer (RamanRXN1, Kaiser Optical Systems, Inc.) via an optic cable. The Raman spectrometer is equipped with a 785 nm laser with 400 mW output power and a charge coupled device detector. Intensity calibration of the Raman spectrometer was performed with a tungsten-halogen reference lamp of the Raman Calibration Accessory (RamanRXN Systems). Cyclohexanol was used for wavenumber calibration and system verification.

In order to prepare the adsorbent for the SE synthesis experiments, the catalyst/adsorbent mixture loaded in the reactor was kept at 250 ^oC for 3 hours under a flow of N_2. The reactor was then

cooled down to the ambient temperature. The catalyst activation was performed by heating the cooled reactor to the point of 250 ^{o}C at a rate of 1 ^{o}C per minute under a flow of H_2 (20 mol.%) balanced with N_2, and then maintaining the reactor under these conditions for additional 90 minutes [53].

Each experiment (**Table 1**) involved 3 consecutive runs of SE methanol synthesis with adsorbent regeneration in between. Considering the highly transient nature of the investigated phenomena, the experimental runs were performed in such a way as to avoid any chemical transformations before the required process conditions are reached. More specifically, the reactor was heated under a constant flow of N_2 to the required temperature. Once the required temperature had been reached, the reactor pressure was gradually increased also under the flow of N_2. After the required process conditions had been reached, the gas analysis system was set, and the experimental run was started by changing the inlet gas composition. All experiments were performed with the constant inlet gas composition: CO_2 – 22.7 mol.%, H_2 – 68.2 mol.%, N_2 – 9.1 mol.%. Each run involved monitoring of the system for at least 30 minutes or until there were no changes in the outlet gas composition for at least 10 consecutive minutes. This approach ensures that by the end of the run the adsorbent is fully saturated, and the SE phase is over. The adsorbent regeneration is achieved by completely depressurizing the reactor and purging it under the flow of N_2 (550 ml_{STP}/min) for 25 minutes while the reactor temperature is maintained at 230 ^{o}C.

For monitoring of the outlet gas composition, Raman spectra were acquired using the exposure time of 45 seconds and a single scan for each spectrum. Concentrations of CO_2, H_2, CO and N_2 were determined directly from the acquired spectral data using a set of reference spectra obtained beforehand. The Raman cell was maintained at ambient pressure and 115 ^{o}C temperature during spectral data acquisition. Methanol concentration was determined by means of the data reconciliation algorithm reported previously [52]. More specifically, the algorithm was applied to determine the methanol concentration value after the adsorbent saturation, i.e. after the SE effect is over and the steady state operation is reached. This value was then coupled with the methanol

signal intensity values acquired from the collected spectral data for a separate SE synthesis run to determine the rest of the methanol concentrations.

2.3. Reactor modeling

A mathematical model (**Appendix A**) was developed to simulate the phenomena occurring in the reactor during the SE methanol synthesis experiments. The phenomenological model consists of a system of partial differential equations (PDEs). The model is one-dimensional, pseudo-homogeneous, non-isothermal, non-adiabatic and non-isobaric. Considering the small diameter of the reactor, the gradients of concentration, velocity, pressure, and temperature are considered negligible in the radial direction. The flow is described by the axial-dispersed plug flow model. The linear driving force model (LDF) is considered for description of the water adsorption kinetics [54]. The changes in the gas flow due to the occurring chemical reactions and adsorption phenomena are considered by the overall mass balance equation. The momentum balance is described using the Darcy's law [41]. The equations forming the basis of the reactor model are provided in **Appendix A** along with a description of the correlations used for estimation of the phenomenological parameters.

The finite difference method is used to spatially discretize the obtained PDEs into a system of coupled ordinary differential equations (ODEs). The first order spatial derivatives (Eqs. A1-A3, A5) are approximated via the five-point upwind finite difference method [55]. The second order spatial derivatives (Eqs. A1, A2, A5, A6) are evaluated via the fourth order approximation algorithm [56]. The spatial discretization is performed by compartmentalizing the simulated adsorbent-catalyst bed into 100 separate sections, each one of which is described by a separate set of ODEs. The obtained system of the coupled ODEs is solved in MATLAB with the standard integration subroutine for stiff problems – 'ode15s' [57].

Several kinetic models describing the process of methanol synthesis exist in the literature [58]. The kinetic model developed by Graaf et al. was developed as a result of a rigorous investigation

of the rate-determining steps of the occurring reactions [59]. The model considers a dual-site Langmuir-Hinshelwood mechanism with dissociative hydrogen adsorption for temperatures in the range between 210 and 275 ^{o}C and pressures up to 50 bar. The model was further improved by the authors taking account of the mass transfer phenomena of the process [60]. A thorough investigation of the chemical equilibria of the reactions was also published [61]. Overall, the research conducted by the authors of the kinetic model has set a significant standard in the context of mathematical modeling of methanol synthesis process.

The kinetic model of VandenBussche and Froment coupling the rates of the CO_2 hydrogenation and RWGS reactions through a surface oxygen intermediate was also widely recognized. The model is developed based on the experimental data acquired at temperatures between 180 and 280 ^{o}C and pressures between 15 and 51 bar [62].

Furthermore, Park et al. reported a new kinetic model for methanol synthesis, which was based upon the assumption of the three-site adsorption. However, the proposed kinetic model was still based on the original kinetic interpretation proposed by Graaf et al. In addition to that, the model also considered formation of DME as a side product [63].

Askgaard et al. also proposed a kinetic model for methanol synthesis by extending their kinetic interpretation of the WGS reaction. All kinetic parameters were estimated from the gas-phase thermodynamics and surface science studies [64].

As methanol is the main product of the process, accurate estimation of its production rate is crucial for a reliable analysis of the SE methanol synthesis process. Therefore, due to its proven accuracy in terms of methanol concentration estimation, demonstrated in our previous study [52], the kinetic model of Graaf et al.[59] was employed for kinetic modeling within the scope of this study. This way, the kinetic rate expressions for the reactions Eqs. 1-3 are given by Eqs. 4-6 respectively:

$$R_1 = \frac{k_1 K_{CO}\left[f_{CO}\sqrt{{f_{H_2}}^3} - \frac{f_{CH_3OH}}{\sqrt{f_{H_2}}K_{p,1}}\right]}{\left(1 + K_{CO}f_{CO} + K_{CO_2}f_{CO_2}\right)\left[\sqrt{f_{H_2}} + \frac{K_{H_2O}}{\sqrt{K_{H_2}}}f_{H_2O}\right]} \quad (4)$$

$$R_2 = \frac{k_2 K_{CO_2}\left[f_{CO_2}f_{H_2} - \frac{f_{H_2O}f_{CO}}{K_{p,2}}\right]}{\left(1 + K_{CO}f_{CO} + K_{CO_2}f_{CO_2}\right)\left[\sqrt{f_{H_2}} + \frac{K_{H_2O}}{\sqrt{K_{H_2}}}f_{H_2O}\right]} \quad (5)$$

$$R_3 = \frac{k_3 K_{CO_2}\left[f_{CO_2}\sqrt{{f_{H_2}}^3} - \frac{f_{CH_3OH}f_{H_2O}}{\sqrt{{f_{H_2}}^3}K_{p,3}}\right]}{\left(1 + K_{CO}f_{CO} + K_{CO_2}f_{CO_2}\right)\left[\sqrt{f_{H_2}} + \frac{K_{H_2O}}{\sqrt{K_{H_2}}}f_{H_2O}\right]} \quad (6)$$

where R_1, R_2 and R_3 are reaction rates per weight of catalyst for reactions 1-3 respectively, mol/(s kg_{cat}); k_1, k_2 and k_3 are the kinetic constants for the same reactions, mol/(s bar kg_{cat}); $K_{p,1}$, $K_{p,2}$ and $K_{p,3}$ are the equilibrium constants for the same reactions; f_i denotes partial fugacity of a component *i*, bar; K_i denotes adsorption constant for a component *i*, bar^{-1}.

Fugacity coefficients for the kinetic equations and the gas mixture compressibility factor were evaluated with the modified Soave-Redlich-Kwong equations of state [65]. The original literature values for the constants used in Eqs. 4-6 are retrieved from [59]. The equilibrium constants are calculated based on the latest reassessment of chemical equilibria in methanol synthesis by [61].

The kinetics of water adsorption onto the 3Å molecular sieve is described with the LDF model [54]:

$$\frac{\partial q_{H_2O}}{\partial t} = k_{LDF}\left(q^*_{H_2O} - q_{H_2O}\right) \quad (7)$$

where q_{H_2O} is adsorbent loading, mol/kg; k_{LDF} is mass transfer coefficient s^{-1}; $q^*_{H_2O}$ is equilibrium adsorbent loading, mol/kg. The expression for calculation of the mass transfer coefficient value is provided in **Appendix A**.

The equilibrium adsorbent loading value for the LDF model is determined with a single-site Langmuir adsorption isotherm model:

$$q^*_{H_2O} = \frac{m_{H_2O} b_{H_2O} y_{H_2O} p}{1 + m_{H_2O} y_{H_2O} p} \quad (8)$$

where m_{H_2O} is the adsorbent saturation capacity, mol/kg; b_{H_2O} is Langmuir adsorption isotherm parameter, Pa^{-1}; y_{H_2O} – water molar fraction; p – reactor pressure, Pa.

2.4. Parameter estimation

It should be noted that in our previous study on methanol synthesis by hydrogenation of pure CO_2 [52] the outlet concentrations of methanol and CO were slightly different from those predicted by the original kinetic model of Graaf et al [59]. It was concluded that with the catalyst used for methanol synthesis, the RWGS reaction was more significant than predicted by the original kinetic model. This discrepancy is caused by the different behavior of the employed catalytic material. The same catalyst was used in this work. Moreover, the experimental data forming the basis of the original kinetic model's parameters have been acquired during steady state experiments in a spinning basket reactor for hydrogenation of mixtures of CO_2 and CO [59]. This work, however, studies the dynamic behavior of methanol synthesis from a stoichiometric mixture of CO_2 and H_2 in a tubular reactor with in-situ water adsorption. Therefore, the parameters characterizing the reaction rates (Eqs. 4-6) and water adsorption (Eq. 8) are estimated in the current work based on the acquired experimental data.

In the rate equations (Eqs. 4-6), the constants describing the rates of the corresponding reactions (k_1, k_2, k_3) are given by the Arrhenius equation in the following way:

$$k_j = A_j \exp\left[-\frac{E_{a,j}}{RT}\right] \quad (9)$$

where: A_j is a pre-exponential factor for kinetic constant of reaction *j*, mol/(s kg_{cat} bar); $E_{a,j}$ is activation energy of reaction *j*, J/mol; R is universal gas constant, J/(mol K); T is reactor temperature, K.

In a similar manner, the components adsorption equilibrium constants $\left(K_{CO}, K_{CO_2}, K_{H_2O}/\sqrt{K_{H_2}}\right)$ are also determined with the Arrhenius type equation:

$$K_i = A_i \exp\left[-\frac{\Delta H_{ads,i}^{cat}}{RT}\right] \tag{10}$$

where: A_i is a pre-exponential factor for *i*-component adsorption equilibrium constant, bar^{-1}; $\Delta H_{ads,i}^{cat}$ is *i*-component heat of adsorption, J/mol.

Likewise, in the equation describing the kinetics of water adsorption onto the molecular sieve (Eq. 8), the Langmuir adsorption isotherm parameter is described in the following way:

$$b_{H_2O} = b_{H_2O,0} \exp\left[-\frac{\Delta H_{ads,H_2O}}{RT}\right] \tag{11}$$

where: $b_{H_2O,0}$ is a Langmuir adsorption isotherm fitting parameter, Pa^{-1}; $\Delta H_{ads,H_2O}$ is heat of water adsorption onto the 3Å molecular sieves, J/mol.

The value for the heat of water adsorption onto the employed sorption material is retrieved from the literature [66] (**Table A1**). This way, overall, there are 14 parameters to be estimated based on the acquired experimental data: 6 pre-exponential factors, 3 activation energy and 3 heat of adsorption values describing the methanol synthesis reactions, the Langmuir adsorption isotherm fitting parameter, and adsorbent saturation capacity (Eq. 8).

The parameter estimation is based upon the values of methanol and CO molar fractions in the reactor outlet stream. The objective function based on the sums of squared residuals is chosen for the parameter estimation. To account for the transient changes in the process performance, the concentration values of methanol and CO are considered for each experiment in the time range

from 2 to 25 minutes of operation. This way, the objective function for the parameter estimation is expressed in the following way:

$$\mathrm{OF} = \sum_{e=1}^{14} \sum_{t=2}^{25} \left[(\hat{y}_{\mathrm{MeOH}} - y_{\mathrm{MeOH}})_{e,t}^2 + (\hat{y}_{\mathrm{CO}} - y_{\mathrm{CO}})_{e,t}^2 \right] \quad (12)$$

where $\hat{y}_{\mathrm{MeOH}}$ and $\hat{y}_{\mathrm{CO}}$ denote the calculated outlet concentration values of methanol and CO respectively, while y_{MeOH} and y_{CO} denote the methanol and CO outlet concentration values determined from the acquired experimental data; index *e* denotes the experiment (**Table 1**); index *t* denotes the time point from the beginning of the SE methanol synthesis process in minutes.

To diminish high parameter correlation between the pre-exponential factors and the corresponding values of activation energy or heat of adsorption during optimization, the Arrhenius type equations for the rate constants are reparametrized in the following form through definition of reference temperature [67]:

$$k = k_{(T_{\mathrm{ref}})} \exp\left[-\frac{B}{R} \left(\frac{1}{T} - \frac{1}{T_{\mathrm{ref}}} \right) \right] \quad (13)$$

where *B* represents either activation energy or heat of adsorption and T_{ref} = 503.15 K.

The objective function is minimized with the interior-point algorithm [68]. The bootstrap method is applied to investigate statistical reliability of the parameter estimation results and evaluate variability of the estimated parameters' values [69]. Considering the immense computational cost of the optimization problem due to significant complexity and non-linearity of the reactor model, the quantity of bootstrap replicates is selected to be 200. Taking into account the statistical basis of the method, the number of the bootstrap replicates may seem low, however, it is considered to be sufficient for a robust estimation of standard error values [70]. Therefore, this number is selected as a tradeoff between accuracy and the amount of time required for the computations.

3. Results and Discussion

The experiments conducted in this study are listed in **Table 1**. No signals of additional products apart from methanol and CO were detected in the acquired spectral data. **Figure 1** demonstrates an example of the C-H stretching region of the acquired Raman spectra. It can be noted that during the SE phase only 4 peaks originating from methanol Raman signal are present in the region [71]. An example of a complete Raman spectra of the reactor outlet stream can be found in the Supporting Information.

During each experiment, production of methanol and CO is significantly enhanced in the beginning of the process due to water adsorption. This results in a significant increase in outlet concentrations of methanol and CO, and decreased outlet concentration of CO_2. As the process continues, the production of methanol and CO gradually decreases due to the fact that the adsorbent is being saturated with water. Consequently, as the time passes, the SE effect, achieved as a result of in-situ water removal, slowly diminishes. Eventually, when the adsorbent is fully saturated, the SE effect is terminated, the water breakthrough point is reached, and the steady state operation is achieved. Raw experimental data, expressed in terms of the main components' signal intensities, can be found in the Supporting Information.

In order to prove that this transient behavior of the system is indeed due to the in-situ water adsorption, a series of additional blank experiments was performed. More specifically, to investigate the transient response of the testing equipment caused by changing the inlet gas composition, a reference experimental run was performed with the reactor filled with inert material. Furthermore, to prove that the observed enhancement in process performance is not associated with any kind of transient catalyst behavior, an additional experiment with the reactor filled only with catalyst was also conducted. In each case, the breakthrough pattern of the outlet components' concentrations was monitored. The acquired experimental data demonstrate that neither the testing equipment nor the employed experimental methodology affect the temporary

increase in the process efficiency recorded during the SE synthesis runs. A more detailed description of the experimental data acquired during these blank experiments is provided in the Supporting Information.

Because of the insufficient accuracy of the standard kinetic model, the experimental observations are compared with the simulation data obtained with the reactor model based on the estimated kinetic parameters. Comparison of the experimentally determined methanol and CO outlet concentrations with the results of the reactor simulation based on the original values of the kinetic parameters can be found in the Supporting Information.

Table 1. Results of the SE methanol synthesis experiments

No	Reactor pressure, bar	Reactor temperature, °C	Catalyst-to-Adsorbent ratio (mass fraction basis)	GHSV, h^{-1} (based on the entire bed volume)	Maximum MeOH outlet concentration, mol.%	MeOH outlet concentration at steady state, mol.%	Maximum CO outlet concentration, mol.%	CO outlet concentration at steady state, mol.%
1	20	230	1:1	2800	1.51	0.97	6.89	2.31
2	30	230	1:1	2800	2.86	1.62	8.69	2.26
3	40	230	1:1	2800	4.98	1.73	10.87	2.23
4	50	230	1:1	2800	5.85	1.82	9.91	2.17
5	60	230	1:1	2800	7.03	2.08	8.77	2.09
6	40	210	1:1	2800	3.93	1.35	5.46	1.55
7	40	250	1:1	2800	5.73	2.04	13.53	2.44
8	40	270	1:1	2800	5.12	1.77	14.86	2.92
9	40	230	1:2	2800	3.51	1.36	9.90	2.16
10	40	230	1:3	2800	2.32	1.09	6.32	1.87
11	40	230	1:4	2800	1.43	0.75	4.16	1.55
12	40	230	2:1	2800	4.63	1.98	9.37	2.15
13	40	230	3:1	2800	4.35	2.24	7.35	2.06
14	40	230	1:1	5600	2.25	1.03	7.98	2.14

Typical reactor effluent concentration profile during the SE methanol synthesis experiments is presented in **Figure 2** both in terms of experimental and simulation data.

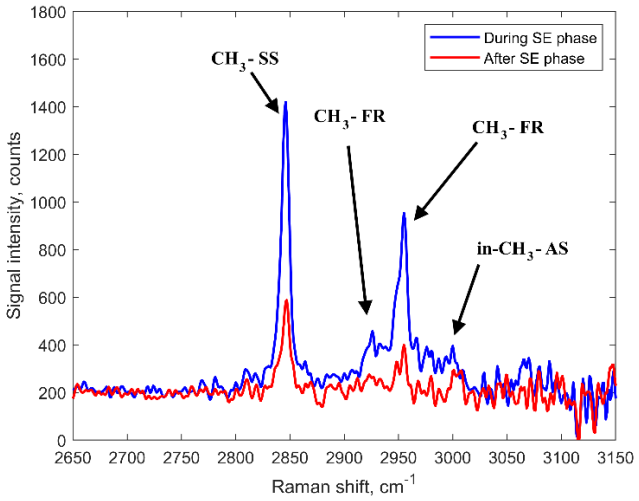

Figure 1. C-H stretching region of the Raman spectra of the reactor outlet stream during and after SE phase

Methanol Raman signal is characterized by the following bands:

CH_3-SS: CH_3 symmetric stretching; CH_3-FR: CH_3 Fermi resonance; in-CH_3-AS: CH_3 antisymmetric stretching;

(the bands assignment is retrieved from [71])

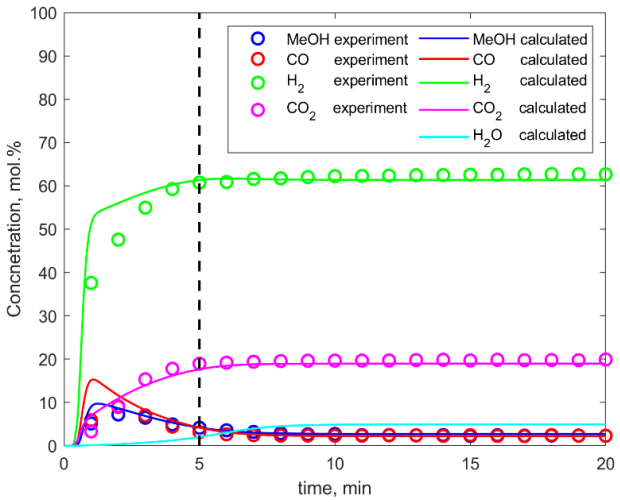

Figure 2. Reactor outlet during SE methanol synthesis experiment (reactor pressure = 60 bar,

temperature = 230 ^{o}C, GHSV = 2800 h^{-1}, catalyst-to-adsorbent ratio = 1:1)

The values of the parameters describing the kinetics of the undergoing reactions and water adsorption obtained from the parameter estimation are provided in **Table 2**. The correlation matrix

proving the absence of the cross-correlation between the estimated kinetic parameters can be found in the Supporting Information along with the histograms depicting the distributions of the parameter values. In general, the values of the estimated parameters are normally distributed. However, estimations of the CO hydrogenation reaction rate constant at reference temperature are skewed towards lower values region, while for the CO_2 adsorption equilibrium constant the distribution bears a rather bimodal pattern. These shortcomings are explicable considering the low number of the bootstrap datasets studied during the parameter estimation. Regardless of these limitations, the obtained results still enable estimation of the validity of the acquired values.

The values of the pre-exponential factors recalculated from the reparametrized equation form (Eq. 13) back to the original context of Arrhenius and Van't Hoff are provided in **Table 3**. Comparison of the kinetic parameters obtained within the limits of this work with the values estimated by Graaf et al. in the context of the kinetic studies of methanol synthesis [59,60] can be found in the Supporting Information (**Table S1**). It should be noted that even though the estimation of the kinetic parameters was performed based on the intrinsic process kinetics, the obtained results are tightly fixed to the process conditions considered within the scope of this work.

The parity plots for methanol and CO outlet concentration values are provided in Figures **3.A-3.B**. Considering the complexity of the system, a reasonably good fit can be observed. The deviations from the diagonal are random and do not exhibit any trends. It can be noted that the deviation is slightly higher in the case of CO outlet concentration values. Due to the high rate of water formation and adsorption, the SE effect propagates through the reactor as a steep front of the components' concentrations. Since the SE effect does not hold for long under the investigated conditions, methanol and CO concentrations at the reactor outlet change drastically within a short period of time. In this context, it is worth highlighting that the analytical Raman probe is installed at some distance from the actual reactor outlet, while the model predicts the concentration values right at the reactor exit. Additionally, between the reactor outlet and the analytical probe a backpressure regulator is installed. More details about the design of the experimental setup can be

found in the Supporting Information. Therefore, the accuracy of the gas composition analysis may have been affected to a minor extent by the axial gas dispersion and the changes in the outlet gas flowrate due to the varying conversion of the initial reactants. In light of this, even though the parity plots provide valuable information about the general goodness of fit, the data depicted there are not perfectly representative in terms of comparison between the calculation results and the experimental observations due to the highly transient nature of the process. This is especially relevant for CO due to the much sharper changes in the outlet concentration values in time. In this sense, the validity of the fitted reactor model should be evaluated based on the overall pattern of the products' outlet concentrations changing in time. More details about this are given further in the text.

Table 2. Estimated parameter values considering the reparameterization of the Arrhenius type equations

Parameter	Value	Standard deviation	Lower limit 95% conf. int.	Upper limit 95% conf. int.
$k_{1\,(T_{\mathrm{ref}})}$, mol/(s kg_{cat} bar)	3.14×10^{-4}	5.14×10^{-5}	3.07×10^{-4}	3.21×10^{-4}
$k_{2\,(T_{\mathrm{ref}})}$, mol/(s kg_{cat} bar)	7.40×10^{-3}	6.29×10^{-4}	7.30×10^{-3}	7.50×10^{-3}
$k_{3\,(T_{\mathrm{ref}})}$, mol/(s kg_{cat} bar)	4.51×10^{-4}	3.37×10^{-5}	4.46×10^{-4}	4.56×10^{-4}
$K_{CO\,(T_{\mathrm{ref}})}$, bar^{-1}	1.28×10^{-2}	1.30×10^{-3}	1.26×10^{-2}	1.30×10^{-2}
$K_{CO_2\,(T_{\mathrm{ref}})}$, bar^{-1}	6.15×10^{-2}	5.30×10^{-3}	6.07×10^{-2}	6.22×10^{-2}
$K_{H_2/H_2O\,(T_{\mathrm{ref}})}$, bar^{-1}	7.66	0.75	7.55	7.77
$E_{a,1}$, J/mol	3.22×10^{4}	1.51×10^{3}	3.20×10^{4}	3.25×10^{5}
$E_{a,2}$, J/mol	6.47×10^{4}	3.16×10^{3}	6.42×10^{4}	6.51×10^{4}
$E_{a,3}$, J/mol	2.52×10^{4}	1.23×10^{3}	2.50×10^{4}	2.54×10^{4}
$\Delta H_{ads,CO}^{cat}$, J/mol	-1.34×10^{4}	622.22	-1.34×10^{4}	-1.32×10^{4}
$\Delta H_{ads,CO_2}^{cat}$, J/mol	-1.26×10^{3}	65.25	-1.27×10^{3}	-1.25×10^{3}
$\Delta H_{ads,H_2/H_2O}^{cat}$, J/mol	-1.01×10^{5}	4.29×10^{3}	-1.02×10^{5}	-9.99×10^{4}
$b_{H_2O\,(T_{\mathrm{ref}})}$, Pa^{-1}	9.47×10^{-6}	1.74×10^{-6}	9.22×10^{-6}	9.73×10^{-6}
m_{H_2O}, mol/kg	3.25	0.19	3.21	3.28

Table 3. Kinetic parameter values calculated from Table 2

Parameter	Value (95% conf. int.)
A_1, mol/(s kg_{cat} bar)	0.8303 (± 4.53×10^{-2})
A_2, mol/(s kg_{cat} bar)	3.24×10^{4} (± 5.21×10^{3})
A_3, mol/(s kg_{cat} bar)	0.1957 (± 8.40×10^{-3})
A_{CO}, bar^{-1}	5.10×10^{-4} (± 1.54×10^{-5})
A_{CO_2}, bar^{-1}	4.90×10^{-2} (± 5.53×10^{-4})
A_{H_2/H_2O}, bar^{-1}	3.18×10^{-10} (± 9.95×10^{-11})
$b_{H_2O,0}$	1.04×10^{-13} (± 2.42×10^{-5})

Although the estimated kinetic parameters are rather different from the parameters proposed by the authors of the original kinetic model [59], the values determined within the scope of this work follow all the physico-chemical constraints. More specifically, the estimated values of activation energies, pre-exponential factors for the reaction rate constants and pre-exponential factors for the adsorption equilibrium constants are positive, while the values of heats of adsorption are negative. Additionally, the negative values of the CO and CO_2 adsorption entropies calculated from the estimated pre-exponential factors for the corresponding adsorption equilibrium constants do not exceed the CO and CO_2 entropies at the process temperature (**Table S2** in the Supporting Information). More detailed description of the physico-chemical constraints can be found elsewhere [62].

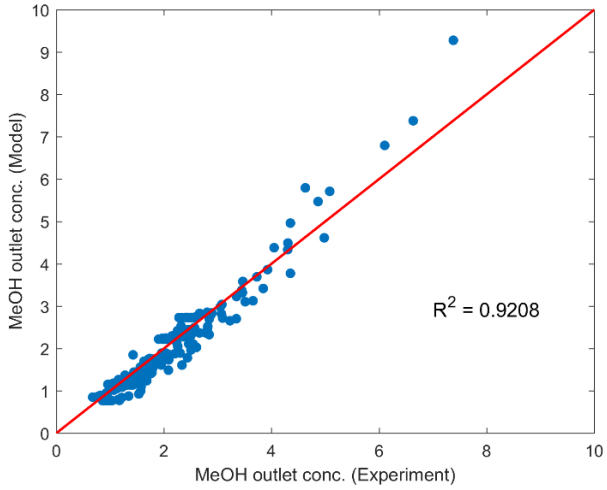

A

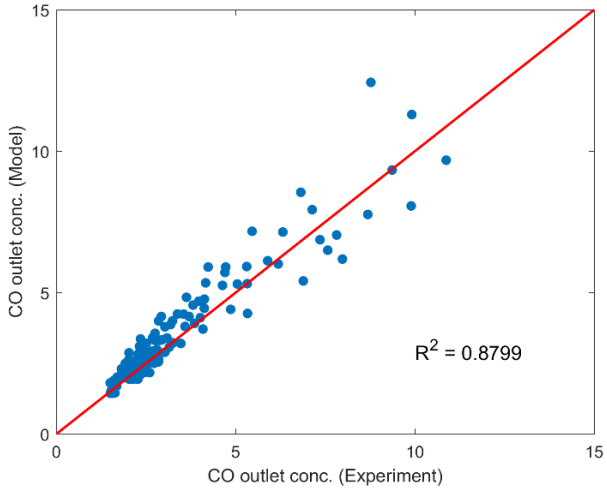

B

Figure 3. Parity plots describing the parameter estimation accuracy

A – outlet methanol concentration values, B – outlet carbon monoxide concentration values

Comparing the rates of the CO and CO_2 hydrogenation reactions (Eqs. 4 and 6 respectively) it can be concluded that the kinetic description based on the estimated values of the kinetic parameters follows the general consensus about CO_2 being the primary carbon source for methanol formation [72]. A graphical representation of the ratio of CO hydrogenation rate to CO_2 hydrogenation rate during the SE methanol synthesis experiments is provided in the Supporting Information for the varying process conditions. It can be noted that in-situ water removal improves the CO hydrogenation reaction more than it does the CO_2 hydrogenation reaction. This is

manifested in increased values of the $R_1:R_3$ ratio during the SE phase of the experiments. This effect is particularly substantial for the increased reactor temperatures. This pattern can also be attributed to the fast kinetics of the RWGS reaction (Eq. 2) during the investigated process. More specifically, the excessive amount of CO, produced due to the fast endothermic RWGS reaction being enhanced as a result of the in-situ water removal, accelerates the CO hydrogenation reaction. After the SE phase, the $R_1:R_3$ ratio is decreased meaning that the rate of the CO hydrogenation reaction is reduced because of the decrease in the CO concentration since the enhancement of the RWGS reaction is over.

It is also worth noting that the value of adsorbent saturation capacity determined in the course of this work is also much lower than those estimated from the data of water adsorption on pure sorptive material without any catalyst [41]. At the same time, the estimated saturation capacity value is in reasonably good agreement with the values of adsorbed water load in SE dimethyl ether synthesis reactor studied by Guffanti et al [38]. In this context, it should be mentioned that to demonstrate the insignificance of competitive adsorption between H_2 and water molecules onto the molecular sieves 3A, the negligible H_2 adsorption onto the adsorbent under the studied process conditions was proven experimentally in the current work. More detailed information about the experiment and the acquired data can be found in the Supporting Information. Although zeolite sorptive materials with 3Å pore diameter exhibit the highest selectivity and affinity towards water molecules, it was previously shown that the presence of methanol species reduces the water uptake capacity of these adsorbents [73,74]. Moreover, in the context of SE processes, it was concluded that water adsorption can be influenced by blockage of the adsorbent pores by the reaction intermediates [75]. In light of these observations, the decreased values of the parameters describing the water adsorption isotherm determined within the limits of this work can be considered reasonable.

A considerable increase of the reactor wall temperature recorded during each experiment should also be mentioned. Particularly, during the SE phase of each experiment, when the produced water is being adsorbed by the molecular sieves, a rapid increase in the reactor temperature can be observed. The temperature rise is due to the exothermicity of the intensified hydrogenation reactions (Eqs. 1 and 3) and the exothermicity of the water adsorption process. As the adsorbent is being saturated with water, and, consequently, the intensification of the occurring chemical reactions is attenuating, the reactor wall temperature steadily decreases. Recorded reactor wall temperature values are provided in the Supporting Information along with the corresponding reactor simulation results. To a minor extent, the recorded reactor wall temperature values were affected by the experimental setup's control system since the setup was not designed to be operated in the adiabatic manner. This way, in general, the agreement between the experimental and simulation results is rather poor. However, it should be noted that the model still accurately estimates the initial temperature rise during the SE phase.

Overall, the obtained experimental data are in good agreement with the observations of Terreni et al. [45], except for the presence of dimethyl ether in the reactor outlet stream. In addition, a more significant increase in CO production during the SE phase of the process as compared with the methanol formation enhancement can also be observed in our experiments. This pattern can be explained by the fact that the rate of the RWGS reaction is more significant under the methanol synthesis conditions studied during this work. In addition to that, it is also worth mentioning that under the process conditions, the RWGS reaction equilibrium constant is ca. 2 orders of magnitude larger than the CO_2 hydrogenation reaction equilibrium constant. The ratio of RWGS equilibrium constant to the CO_2 hydrogenation equilibrium constant during and after the SE phase is provided in the Supporting Information. It can be noted that, because of the significant production of heat during the SE phase, the RWGS reaction becomes more thermodynamically favorable.

3.1. Experiments with varied reactor pressure

Outlet concentrations of methanol and CO during the SE methanol synthesis experiments with varied reactor pressure are provided in **Figures 4.A-4.B** both in terms of experimental observations and process simulation results. In good agreement with the Le Chatelier's principle, the increase in reactor pressure improves methanol production and CO_2 conversion. However, it is also worth noting that the increase in the reactor pressure also increases the significance of the SE effect in terms of methanol production. At the same time, the effect of the increase in reactor pressure on CO production during the SE phase is quite the opposite. More specifically, the acquired experimental data indicates that CO production decreases when the reactor pressure exceeds 40 bar. This means, that under the process conditions, the hydrogenation reactions (Eqs. 1 and 3), which involve reduction in the total number of moles, become more significant than the RWGS reaction (Eq. 2) because of the pressure increase. This way, methanol formation is improved while CO concentration in the outlet is decreased. Thus, it can be concluded that more CO is converted to methanol at higher pressures via the CO hydrogenation reaction (Eq. 1).

The outlet concentration data might not give enough information about methanol production rate because of the decrease in the gas flowrate as a result of the reduction in the total number of moles due to the hydrogenation reactions (Eqs. 1 and 3). Therefore, specific methanol production rates retrieved from the reactor model based on the estimated kinetic parameters can be found in the Supporting Information.

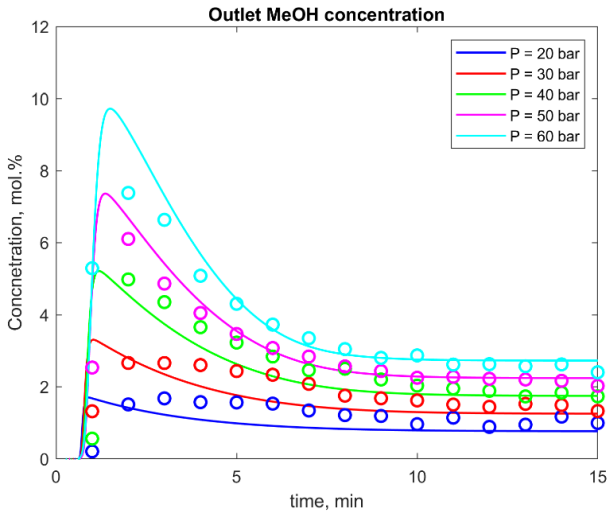

A

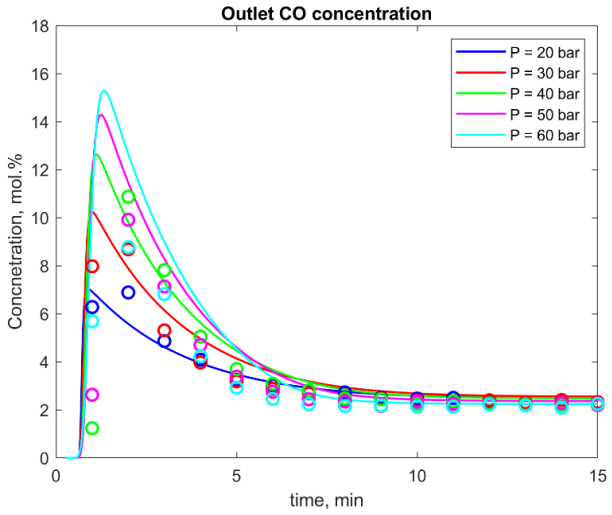

B

Figure 4. Outlet concentrations during SE methanol synthesis for the experiments with varied reactor pressure

A – methanol concentration, B – carbon monoxide concentration

reactor temperature = 230ºC, catalyst-to-adsorbent ratio = 1:1, GHSV = 2800 h^{-1}

solid lines denote process simulation results; circles represent experimental observations;

Even though the agreement between the experimental and simulated values of methanol and CO concentrations is reasonably good for the major part, the model is not able to predict the decrease in CO outlet concentration at the elevated reactor pressure. This minor drawback is explicable considering the high non-linearity of the system of PDEs employed for the process simulation and

substantial complexity of the optimization problem during parameter estimation. Alongside with that, it should be also noted that the model does predict the decrease in the enhancement of CO production during SE phase as the reactor pressure rises. Additionally, the steady state concentration values of CO after the SE phase are also estimated reasonably accurately.

Since the increase in the reactor pressure results in higher methanol and CO production during the SE phase, the conversion of CO_2 and H_2 is also much higher in the beginning of the process. Outlet concentration profiles of the initial reactants during the SE synthesis runs are provided in the Supporting Information. As the reactor pressure rises, the components reach the steady state outlet concentration values much slower. This way, the curves, describing CO_2 and H_2 outlet concentrations during the SE phase, flatten with the reactor pressure increase, indicating higher conversion.

3.2. Experiments with varied reactor temperature

Outlet concentrations of methanol and CO during the SE methanol synthesis experiments with varied reactor temperature are provided in **Figures 5.A-5.B** both in terms of experimental observations and process simulation results. The effect of reactor temperature on the SE methanol synthesis process is rather similar to its effect on the conventional methanol synthesis process.

Initially, as the reactor temperature rises, the methanol production is improved due to increase in the rate of the occurring chemical reactions. However, when the reactor temperature exceeds 250 ^{o}C, the exothermic hydrogenation reactions (Eqs. 1 and 3) face the thermodynamic equilibrium and, thus, the methanol formation is suppressed. At the same time, the effect of temperature is more straightforward in terms of CO production. Since CO can only be produced through the endothermic RWGS reaction, increased reactor temperature drastically improves formation of CO. Moreover, the higher the reactor temperature, the more significant the SE effect on CO formation is. Exothermic reaction of CO hydrogenation to methanol is also suppressed

under the increased temperature conditions, which also increases CO concentration in the product stream at elevated process temperatures.

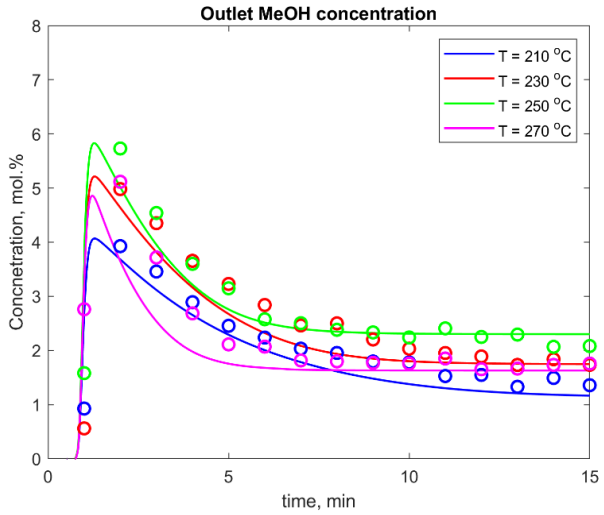

A

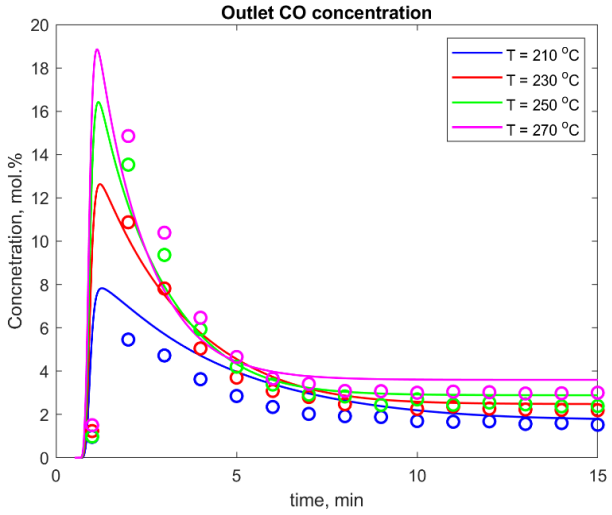

B

Figure 5. Outlet concentrations during SE methanol synthesis for the experiments with varied reactor temperature

A – methanol concentration, B – carbon monoxide concentration

reactor pressure = 40 bar, catalyst-to-adsorbent ratio = 1:1, GHSV = 2800 h^{-1}

solid lines denote process simulation results; circles represent experimental observations;

It is also worth noting that the duration of the SE effect is shorter for the experiments with high reactor temperature. It can be explained by the fact that high temperature is not favorable for

adsorption processes. This way, increased reactor temperature decreases the overall water uptake by the adsorbent, thus making the SE effect last shorter. Another issue is that increased rate of RWGS reaction also results in enhanced water formation, which, in turn, results in rapid adsorbent saturation. These changes in the SE effect duration are particularly evident in terms of methanol production rates (the Supporting Information). A point that should be highlighted here is that even though the maximum methanol formation rate is still observed at 250 ^{o}C, better performance in terms of the SE phase duration can be noted for 210 ^{o}C and 230 ^{o}C reactor temperatures.

Comparing the experimental values of CO and methanol outlet concentrations with the predictions of the reactor model based on the original kinetic parameters (the Supporting Information) it can be observed that methanol and CO formation is much higher at lower temperatures than estimated by the original kinetic model. These observations substantiate the decreased activation energy values estimated within the limits of this work.

The changes in the process performance due to the variation in the reactor temperature can also be observed in the H_2 and CO_2 outlet concentration profiles (the Supporting Information). More specifically, the rate at which H_2 and CO_2 reach the steady-state outlet concentrations increases considerably as the reactor temperature rises, indicating the shortening of the SE phase duration due to faster saturation of the adsorbent and its lower capacity at the elevated temperatures.

3.3. Experiments with varied bed composition

Outlet concentrations of methanol and CO during the SE methanol synthesis experiments with varied reactor bed composition are provided in **Figures 6.A-6.B** both in terms of experimental observations and process simulation results. The variation in the catalyst-to-adsorbent ratio in the SE methanol synthesis experiments affects both methanol and CO production rates in a similar manner. From the obtained data it can be noted that the increase in the adsorbent loading results in a slight increase in the SE phase duration, since the overall amount of water that can be removed from the system is increased. It is worth mentioning that the overall bed volume was maintained

constant during these experiments, and the increase in the adsorbent loading comes at the cost of reducing the amount of catalyst in the reactor. This way, production of methanol and CO is greatly reduced because there is much less catalyst loaded in the reactor. Therefore, the actual GHSV value in terms of the contact time with the catalyst is much lower. This results in a significant decrease of the overall conversion and has a particularly detrimental impact on methanol production after the SE phase. This pattern can also be observed in the CO_2 and H_2 outlet concentration profiles for these experiments (Supporting Information), which bear considerable commonalities with the same results for the experiments with varied reactor temperature, in terms of the SE phase duration. In this context it is also worth mentioning that CO outlet concentrations after the SE phase are not affected by this decrease in the overall conversion as significantly as methanol outlet concentrations. This observation also corroborates the notion about RWGS being much faster than the hydrogenation reactions, which aligns well with the estimated kinetic parameter values.

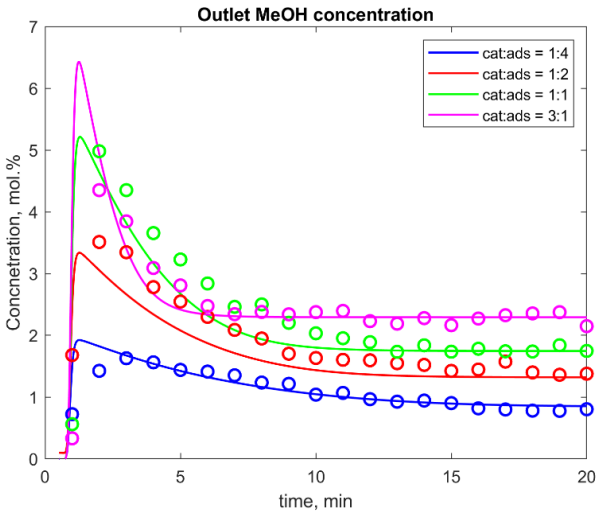

A

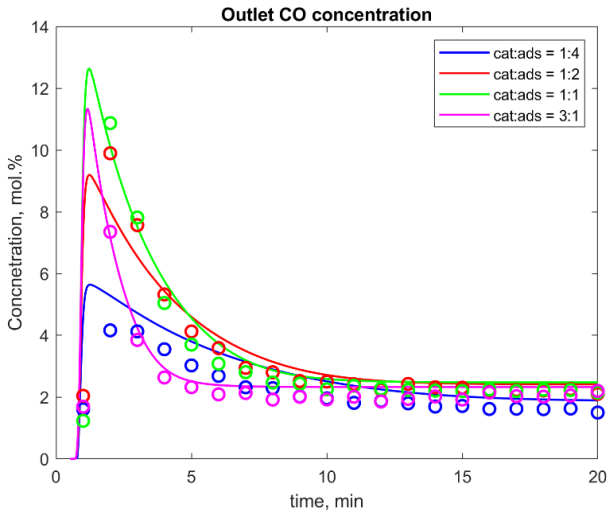

B

Figure 6. Outlet concentrations during SE methanol synthesis for the experiments with varied bed composition

A – methanol concentration, B – carbon monoxide concentration

reactor pressure = 40 bar, reactor temperature = 230ºC, GHSV = 2800 h^{-1}

solid lines denote process simulation results; circles represent experimental observations;

The increase in the amount of catalyst loaded in the reactor comes at the cost of reduced adsorbent amount. Therefore, the SE effect holds for a much shorter period of time, which can be observed from both methanol and CO outlet concentration profiles. However, the peak in production of both methanol and CO due to water removal is much more significant. With the experimental setup employed in this work, the time resolution of the outlet gas composition monitoring was limited to 1 analysis per minute. Therefore, the sharp peak in the products' formation during the SE phase of the experiment with 3:1 catalyst-to-adsorbent ratio was not verified experimentally. Additionally, with such a sharp peak in methanol production during the experiment, it is also possible that the accuracy of the components' concentrations measurement was affected by the aforementioned minor limitations of the experimental setup.

3.4. Experiments with varied flowrate

Outlet concentrations of methanol and CO during the SE methanol synthesis experiments with varied values of the overall gas flowrate are provided in **Figures 7.A-7.B** both in terms of experimental observations and process simulation results. Increased overall gas flowrate decreases methanol outlet concentration. The duration of the SE phase is also slightly reduced with increased GHSV. This reduction is explained by the fact that, because of its high rate, the RWGS rection is more prevalent under the increased GHSV conditions compared to the hydrogenation reactions. This is supported by the fact that outlet CO concentration after the SE phase remains practically unchanged for both experiments. Therefore, since under these conditions the RWGS reaction is more significant, the thermodynamic equilibrium shift, achieved because of the selective water removal, in turn, enhances water formation in a more substantial way compared with methanol formation. Consequently, the adsorbent is saturated much faster, which shortens the duration of the SE phase. This decrease in the SE phase duration is also demonstrated by the H_2 and CO_2 outlet concentration profiles during the experiments (the Supporting Information). As for the steady state operation after complete adsorbent saturation, the obtained results are rather similar to the observations explained for the experiments with varied reactor bed composition.

However, although outlet methanol concentrations are lower for the increased GHSV experiment, the methanol production is much higher in this case due to the higher gas flowrate (the Supporting Information). The differences in the SE phase duration are also more evident in terms of the methanol production values.

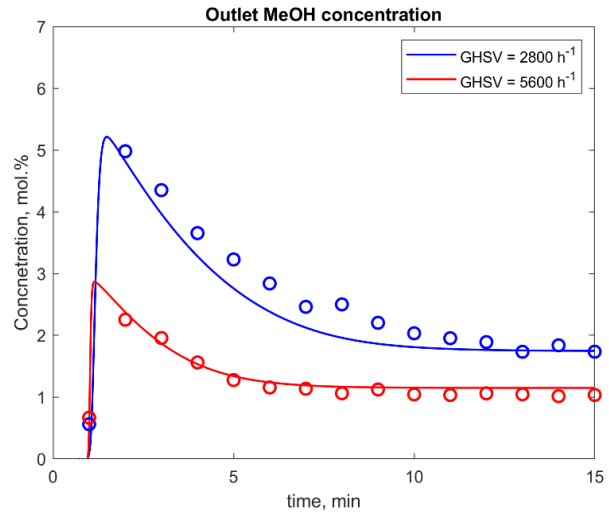

A

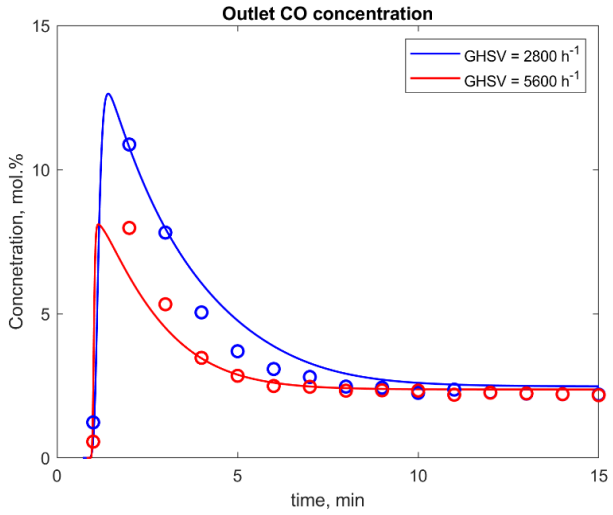

B

Figure 7. Outlet concentrations during SE methanol synthesis for the experiments with varied GHSV

A – methanol concentration, B – carbon monoxide concentration

reactor pressure = 40 bar, reactor temperature = 230°C, catalyst-to-adsorbent ratio = 1:1

solid lines denote process simulation results; circles represent experimental observations;

4. Conclusions

A thorough experimental verification of the concept of methanol synthesis through SE hydrogenation of pure CO_2 is conducted in this work. For better understanding of the involved phenomena, a dynamic pseudo-homogeneous one-dimensional model of the process is developed. The effect of process parameters such as reactor pressure, temperature, overall gas flowrate and catalyst-to-adsorbent ratio on the process performance is addressed. Taking into account the differences between the analyzed system and conventional methanol synthesis studies, the parameters describing kinetics of the occurring reactions and water adsorption are adjusted to fit the acquired experimental data.

A significant temporary improvement in process efficiency, achieved as a result of in-situ water removal, is reported. Particularly, depending on the process conditions, methanol outlet concentration during the SE phase is ca. 150-290 % of the steady state values recorded after the complete adsorbent saturation. For CO, this enhancement factor is ca. 220-510 %. The increase in methanol and CO production during the SE phase is accompanied by the corresponding increase in CO_2 and H_2 conversion.

Reactor pressure is demonstrated to have the most significant impact on the enhancement of methanol production rate during the SE phase. Moreover, the acquired experimental data indicates that increasing reactor pressure above 40 bar improves methanol formation at the cost of reducing CO production, thus greatly improving the process selectivity during the SE phase. Although the increase in reactor pressure considerably improves methanol formation intensity, the duration of the SE phase remains practically unchanged. The increase in the reactor temperature, on the other hand, not only affects the methanol and CO production rates, but also notably shortens the SE phase duration. Even though, initially, increasing reactor temperature improves the process performance due to faster reaction kinetics, methanol formation during the SE phase is substantially suppressed at temperatures above 250 ^{o}C, while CO production rate steadily increases

as the reactor temperature rises. The changes in the overall gas flowrate and the composition of the catalyst:adsorbent mixture affect production of methanol to a much greater extent than CO because of the faster kinetics of RWGS reaction.

Although the relatively short duration of the SE effect reported in this work might seem discouraging in the context of the potential industrial applicability of the SE CO_2 hydrogenation concept, it should be noted that this issue can be improved by adjusting the GHSV. This way, with lower gas flowrates and increased reactor size, the duration and effectiveness of the SE effect can be tremendously improved thus making the process more practical. Additionally, application of sorption materials that would be able to selectively uptake larger amounts of water at elevated temperatures without intervening with the process chemistry is also of great economic interest. It is also worth mentioning that with the system described within the scope of the work, methanol is the only liquid product in the reactor outlet during the SE phase of the process, which significantly simplifies downstream processing.

Acknowledgements

The work was supported by ERDF European Regional Development Fund Grant no. A74130

Appendix A. Reactor model governing equations

The mass balance for component i (except for $i = H_2O$) [76]:

$$\frac{\partial y_i}{\partial t} = \frac{y_i}{T}\frac{\partial T}{\partial t} - \frac{y_i}{p}\frac{\partial p}{\partial t} + D_l\frac{\varepsilon_b}{\varepsilon_t}\frac{T}{P}\frac{\partial}{\partial z}\left(\frac{p\partial y_i}{T\partial z}\right) - \frac{\varepsilon_b}{\varepsilon_t}\frac{T}{p}\frac{\partial}{\partial z}\left(\frac{y_i vp}{T}\right) - \frac{\rho_{cat}RT}{\varepsilon_t p}\sum_{j\in R}\vartheta_{i,j}\,\eta_j\left(-R_j\right) \quad \text{(A1)}$$

The mass balance equation for H_2O species is:

$$\frac{\partial y_{H_2O}}{\partial t} = \frac{y_{H_2O}}{T}\frac{\partial T}{\partial t} - \frac{y_{H_2O}}{p}\frac{\partial p}{\partial t} + D_l\frac{\varepsilon_b}{\varepsilon_t}\frac{T}{p}\frac{\partial}{\partial z}\left(\frac{p\partial y_{H_2O}}{T\partial z}\right) - \frac{\varepsilon_b}{\varepsilon_t}\frac{T}{p}\frac{\partial}{\partial z}\left(\frac{y_{H_2O}vp}{T}\right)$$
$$- \frac{\rho_{cat}RT}{\varepsilon_t p}\sum_{j\in R}\vartheta_{H_2O,j}\,\eta_k\left(-R_j\right) - \frac{\rho_{ads}RT}{\varepsilon_t p}\frac{\partial q_{H_2O}}{\partial t} \quad \text{(A2)}$$

The overall mass balance equation:

$$\frac{\partial p}{\partial t} = \frac{y_i}{T}\frac{\partial p}{\partial t} - \frac{\varepsilon_b}{\varepsilon_t}\frac{T}{p}\frac{\partial}{\partial z}\left(\frac{vp}{T}\right) - \frac{\rho_{cat}RT}{\varepsilon_t p}\sum_{i\in I}\sum_{j\in R}\vartheta_{i,j}\,n_j\left(-R_j\right) - \frac{\rho_{ads}RT}{\varepsilon_t p}\frac{\partial q_{H_2O}}{\partial t} \quad \text{(A3)}$$

The axial pressure drop is described by the Darcy's law [42]:

$$-\frac{\partial p}{\partial z} = \frac{150}{4{r_p}^2}\left(\frac{1-\varepsilon_t}{\varepsilon_t}\right)^2\mu v \quad \text{(A4)}$$

The overall energy balance for the catalyst/adsorbent mixture bed is formulated as [42,76]:

$$\left(\rho_{ads}C_{p,ads} + \rho_{cat}C_{p,cat} + \rho_{ads}C_{p,H_2O}q_{H_2O}\right)\frac{\partial T}{\partial t} = k_z\frac{\partial^2 T}{\partial z^2} - \frac{C_{p,g}\varepsilon_b}{R}\frac{\partial(vp)}{\partial z}$$
$$+\rho_{ads}\left(-\Delta H_{ads,H_2O}\right)\frac{\partial q_{H_2O}}{\partial t} + \rho_{cat}\sum_{j\in R}\eta_j R_j\left(-\Delta H_{R,j}\right) - \frac{2h_{in}}{r_{in}}\left(T - T_w\right) \quad \text{(A5)}$$

The energy balance for the reactor wall element is described as [42]:

$$\rho_w C_{p,w}\frac{\partial T_w}{\partial t} = k_w\frac{\partial^2 T_w}{\partial z^2} + \frac{2r_{in}h_{in}(T - T_w)}{({r_{out}}^2 - {r_{in}}^2)} - \frac{2r_{out}h_{out}(T_w - T_{out})}{({r_{out}}^2 - {r_{in}}^2)} \quad \text{(A6)}$$

The mass transfer coefficient value for the LDF model is determined with the following expression:

$$\frac{1}{k_{LDF}} = \left(\frac{r_p}{3k_f} + \frac{{r_p}^2}{15D_p}\right)\frac{q_{H_2O}\rho_{ads,p}\,RT}{y_{H_2O}p} + \frac{{r_c}^2}{15D_c} \quad \text{(A7)}$$

The gas mixture viscosity and thermal conductivity were estimated with the correlations developed by Chung, et al. [77]. The values of acentric factors and critical volumes for the components were retrieved from [78]. The packed bed axial thermal conductivity was determined with the correlation developed by Yegi, et al. [79]. The heat transfer coefficient value was estimated with the correlations developed by Li and Finlayson [80]. The values of the diffusion coefficients were determined by the equations developed by Fuller, et al. [81]. In order to take the mass transfer phenomena into consideration, the values of the reactions' effectiveness factors were estimated through the Thiele modulus in accordance with the data reported by Lommerts, et al. [82]. The axial diffusion coefficient value was determined with the correlations reported by Edwards and Richardson [83]. Evaluation of the film mass transfer coefficient value was done through calculation of the dimensionless Sherwood, Schmidt, and Reynolds numbers [54]. The constants used for the model equations are provided in Table A1.

Table A1. Constants for the phenomenological reactor model

Parameters	Value	Ref.
$\rho_{cat,p}$ – catalyst pellet density, kg/m^3	1450	This work
$\rho_{ads,p}$ – adsorbent pellet density, kg/m^3	625	This work
r_p – average particle radius, m	2×10^{-4}	This work
D_p – macropore diffusivity, m^2/s	3×10^{-5}	[84]
D_c – micropore diffusivity, m^2/s	3×10^{-7}	[42]
$C_{p,ads}$ – adsorbent heat capacity, J/(kg·K)	1045	[66]
$C_{p,cat}$ – catalyst heat capacity, J/(kg·K)	850	[42]
ε_b – bed porosity;	0.34	This work
ε_p – particle porosity;	0.28	This work
ε_t – total porosity;	0.52	This work
$\Delta H_{ads,H_2O}$ – heat of water adsorption on the adsorbent kJ/(mol);	78	[66]

References

[1] D. Azhgaliyeva, Energy storage and renewable energy deployment: Empirical Evidence from OECD countries, in: Energy Procedia, 2019. https://doi.org/10.1016/j.egypro.2019.01.897.

[2] G. Centi, E.A. Quadrelli, S. Perathoner, Catalysis for CO2 conversion: A key technology for rapid introduction of renewable energy in the value chain of chemical industries, Energy Environ. Sci. (2013). https://doi.org/10.1039/c3ee00056g.

[3] J. Klankermayer, W. Leitner, Harnessing renewable energy with CO2 for the chemical value chain: Challenges and opportunities for catalysis, Philos. Trans. R. Soc. A Math. Phys. Eng. Sci. (2016). https://doi.org/10.1098/rsta.2015.0315.

[4] H.H. Kung, Methanol Production and Use, Marcel Dekker, New York, 1994.

[5] G.A. Olah, Beyond oil and gas: The methanol economy, Angew. Chemie - Int. Ed. (2005). https://doi.org/10.1002/anie.200462121.

[6] U. Bossel, B. Eliasson, G. Taylor, The Future of the Hydrogen Economy: Bright or Bleak?, Cogener. Compet. Power J. (2003). https://doi.org/10.1080/15453660309509023.

[7] A. Kätelhön, R. Meys, S. Deutz, S. Suh, A. Bardow, Climate change mitigation potential of carbon capture and utilization in the chemical industry, Proc. Natl. Acad. Sci. U. S. A. (2019). https://doi.org/10.1073/pnas.1821029116.

[8] Fiedler Eckhard, G. Georg, Kersebohm D. Burkhard, W. Gunther, W. Claus, Methanol, in: Ullmann'S Encycl. Ind. Chem., Wiley-VCH Verlag GmbH & Co. KGaA, Weinheim, 2007.

[9] A. Tremel, P. Wasserscheid, M. Baldauf, T. Hammer, Techno-economic analysis for the synthesis of liquid and gaseous fuels based on hydrogen production via electrolysis, in: Int.

J. Hydrogen Energy, 2015. https://doi.org/10.1016/j.ijhydene.2015.01.097.

[10] K.R. Westerterp, M. Kuczynski, C.H.M. Kamphuis, Synthesis of Methanol in a Reactor System with Interstage Product Removal, Ind. Eng. Chem. Res. (1989). https://doi.org/10.1021/ie00090a018.

[11] J.C.J. Bart, R.P.A. Sneeden, Copper-zinc oxide-alumina methanol catalysts revisited, Catal. Today. (1987). https://doi.org/10.1016/0920-5861(87)80001-9.

[12] F. Arena, K. Barbera, G. Italiano, G. Bonura, L. Spadaro, F. Frusteri, Synthesis, characterization and activity pattern of Cu-ZnO/ZrO2 catalysts in the hydrogenation of carbon dioxide to methanol, J. Catal. (2007). https://doi.org/10.1016/j.jcat.2007.04.003.

[13] O.S. Joo, K.D. Jung, I. Moon, A.Y. Rozovskii, G.I. Lin, S.H. Han, S.J. Uhm, Carbon dioxide hydrogenation to form methanol via a reverse-water-gas- shift reaction (the CAMERE process), Ind. Eng. Chem. Res. (1999). https://doi.org/10.1021/ie9806848.

[14] X.M. Liu, G.Q. Lu, Z.F. Yan, J. Beltramini, Recent Advances in Catalysts for Methanol Synthesis via Hydrogenation of CO and CO2, Ind. Eng. Chem. Res. (2003). https://doi.org/10.1021/ie020979s.

[15] J. Ma, N. Sun, X. Zhang, N. Zhao, F. Xiao, W. Wei, Y. Sun, A short review of catalysis for CO2 conversion, Catal. Today. (2009). https://doi.org/10.1016/j.cattod.2009.08.015.

[16] M. Sahibzada, I.S. Metcalfe, D. Chadwick, Methanol synthesis from CO/CO2/H2 over Cu/ZnO/Al2O3 at differential and finite conversions, J. Catal. (1998). https://doi.org/10.1006/jcat.1998.1964.

[17] K. Fujimoto, Y. Yu, Spillover effect on the stabilization of Cu-Zn catalyst for CO2 hydrogenation to methanol, Stud. Surf. Sci. Catal. (1993). https://doi.org/10.1016/S0167-2991(08)63219-X.

[18] O. Martin, J. Pérez-Ramírez, New and revisited insights into the promotion of methanol synthesis catalysts by CO2, Catal. Sci. Technol. (2013). https://doi.org/10.1039/c3cy00573a.

[19] J.T. Sun, I.S. Metcalfe, M. Sahibzada, Deactivation of Cu/ZnO/Al2O3 methanol synthesis catalyst by sintering, Ind. Eng. Chem. Res. (1999). https://doi.org/10.1021/ie990078s.

[20] M.B. Fichtl, D. Schlereth, N. Jacobsen, I. Kasatkin, J. Schumann, M. Behrens, R. Schlögl, O. Hinrichsen, Kinetics of deactivation on Cu/ZnO/Al2O3 methanol synthesis catalysts, Appl. Catal. A Gen. (2015). https://doi.org/10.1016/j.apcata.2015.06.014.

[21] A. Riaz, G. Zahedi, J.J. Klemeš, A review of cleaner production methods for the manufacture of methanol, J. Clean. Prod. (2013). https://doi.org/10.1016/j.jclepro.2013.06.017.

[22] J.G. Sanchez Marcano, T.T. Tsotsis, Catalytic Membranes and Membrane Reactors, 2002. https://doi.org/10.1002/3527601988.

[23] R.P.W.J. Struis, S. Stucki, M. Wiedorn, A membrane reactor for methanol synthesis, J. Memb. Sci. (1996). https://doi.org/10.1016/0376-7388(95)00222-7.

[24] R.P.W.J. Struis, S. Stucki, Verification of the membrane reactor concept for the methanol synthesis, Appl. Catal. A Gen. (2001). https://doi.org/10.1016/S0926-860X(01)00548-8.

[25] G. Chen, Q. Yuan, Methanol synthesis from CO2 using a silicone rubber/ceramic composite membrane reactor, Sep. Purif. Technol. (2004). https://doi.org/10.1016/S1383-5866(03)00195-3.

[26] J.G. van Bennekom, R.H. Venderbosch, J.G.M. Winkelman, E. Wilbers, D. Assink, K.P.J. Lemmens, H.J. Heeres, Methanol synthesis beyond chemical equilibrium, Chem. Eng. Sci. (2013). https://doi.org/10.1016/j.ces.2012.10.013.

[27] M.J. Bos, D.W.F. Brilman, A novel condensation reactor for efficient CO2 to methanol conversion for storage of renewable electric energy, Chem. Eng. J. (2015). https://doi.org/10.1016/j.cej.2014.10.059.

[28] J. Reichert, S. Maerten, K. Meltzer, A. Tremel, M. Baldauf, P. Wasserscheid, J. Albert, Shifting the equilibrium of methanol synthesis from CO2 by: In situ absorption using ionic liquid media, Sustain. Energy Fuels. (2019). https://doi.org/10.1039/c9se00494g.

[29] B.T. Carvill, J.R. Hufton, M. Anand, S. Sircar, Sorption-Enhanced Reaction Process, AIChE J. (1996). https://doi.org/10.1002/aic.690421008.

[30] A. Borgschulte, N. Gallandat, B. Probst, R. Suter, E. Callini, D. Ferri, Y. Arroyo, R. Erni, H. Geerlings, A. Züttel, Sorption enhanced CO2 methanation, Phys. Chem. Chem. Phys. (2013). https://doi.org/10.1039/c3cp51408k.

[31] I. Aloisi, A. Di Giuliano, A. Di Carlo, P.U. Foscolo, C. Courson, K. Gallucci, Sorption enhanced catalytic Steam Methane Reforming: Experimental data and simulations describing the behaviour of bi-functional particles, Chem. Eng. J. (2017). https://doi.org/10.1016/j.cej.2016.12.014.

[32] A. Di Giuliano, K. Gallucci, F. Giancaterino, C. Courson, P.U. Foscolo, Multicycle sorption enhanced steam methane reforming with different sorbent regeneration conditions: Experimental and modelling study, Chem. Eng. J. (2019). https://doi.org/10.1016/j.cej.2018.09.035.

[33] K.F. Tzanetis, C.S. Martavaltzi, A.A. Lemonidou, Comparative exergy analysis of sorption enhanced and conventional methane steam reforming, in: Int. J. Hydrogen Energy, 2012. https://doi.org/10.1016/j.ijhydene.2012.02.191.

[34] A.N. Antzaras, E. Heracleous, A.A. Lemonidou, Sorption enhanced–chemical looping steam methane reforming: Optimizing the thermal coupling of regeneration in a fixed bed

reactor, Fuel Process. Technol. 208 (2020) 106513. https://doi.org/https://doi.org/10.1016/j.fuproc.2020.106513.

[35] J. Boon, K. Coenen, E. van Dijk, P. Cobden, F. Gallucci, M. van Sint Annaland, Sorption-Enhanced Water–Gas Shift, in: Adv. Chem. Eng., 2017. https://doi.org/10.1016/bs.ache.2017.07.004.

[36] Y. Ju, H.-T. Oh, J.-C. Lee, C.-H. Lee, Performance and dynamic behavior of sorption-enhanced water-gas shift reaction in a fluidized bed reactor for H2 production and CO2 capture, Chem. Eng. J. (2020) 127414. https://doi.org/https://doi.org/10.1016/j.cej.2020.127414.

[37] Y. Hu, H. Cui, Z. Cheng, Z. Zhou, Sorption-enhanced water gas shift reaction by in situ CO2 capture on an alkali metal salt-promoted MgO-CaCO3 sorbent, Chem. Eng. J. (2019). https://doi.org/10.1016/j.cej.2018.08.209.

[38] S. Guffanti, C. Giorgio Visconti, J. van Kampen, J. Boon, G. Groppi, Reactor modelling and design for sorption enhanced dimethyl ether synthesis, Chem. Eng. J. (2020). https://doi.org/10.1016/j.cej.2020.126573.

[39] J. Van Kampen, J. Boon, J. Vente, M. Van Sint Annaland, Sorption enhanced dimethyl ether synthesis for high efficiency carbon conversion: Modelling and cycle design, J. CO2 Util. (2020). https://doi.org/10.1016/j.jcou.2019.12.021.

[40] D. Liuzzi, C. Peinado, M.A. Peña, J. van Kampen, J. Boon, S. Rojas, Increasing dimethyl ether production from biomass-derived syngas via sorption enhanced dimethyl ether synthesis , Sustain. Energy Fuels. (2020). https://doi.org/10.1039/d0se01172j.

[41] A. Arora, S.S. Iyer, I. Bajaj, M.M. Faruque Hasan, Optimal Methanol Production via Sorption-Enhanced Reaction Process, Ind. Eng. Chem. Res. (2018). https://doi.org/10.1021/acs.iecr.8b02543.

[42] A. Arora, S.S. Iyer, M.M.F. Hasan, GRAMS: A general framework describing adsorption, reaction and sorption-enhanced reaction processes, Chem. Eng. Sci. (2018). https://doi.org/10.1016/j.ces.2018.07.031.

[43] M. Bayat, M. Hamidi, Z. Dehghani, M.R. Rahimpour, A. Shariati, Hydrogen/methanol production in a novel multifunctional reactor with in situ adsorption: Modeling and optimization, Int. J. Energy Res. (2014). https://doi.org/10.1002/er.3092.

[44] M. Bayat, Z. Dehghani, M. Hamidi, M.R. Rahimpour, Methanol synthesis via sorption-enhanced reaction process: Modeling and multi-objective optimization, J. Taiwan Inst. Chem. Eng. (2014). https://doi.org/10.1016/j.jtice.2013.06.013.

[45] J. Terreni, M. Trottmann, T. Franken, A. Heel, A. Borgschulte, Sorption-Enhanced Methanol Synthesis, Energy Technol. (2019). https://doi.org/10.1002/ente.201801093.

[46] H. Nieminen, G. Givirovskiy, A. Laari, T. Koiranen, Alcohol promoted methanol synthesis enhanced by adsorption of water and dual catalysts, J. CO2 Util. (2018). https://doi.org/10.1016/j.jcou.2018.01.002.

[47] N. Mehio, S. Dai, D.E. Jiang, Quantum mechanical basis for kinetic diameters of small gaseous molecules, J. Phys. Chem. A. (2014). https://doi.org/10.1021/jp412588f.

[48] C.A. Scholes, S.E. Kentish, G.W. Stevens, Carbon Dioxide Separation through Polymeric Membrane Systems for Flue Gas Applications, Recent Patents Chem. Eng. (2008).

[49] J. van Kampen, J. Boon, M. van Sint Annaland, Steam adsorption on molecular sieve 3A for sorption enhanced reaction processes, Adsorption. (2020). https://doi.org/10.1007/s10450-020-00283-8.

[50] E. Gabruś, J. Nastaj, P. Tabero, T. Aleksandrzak, Experimental studies on 3A and 4A zeolite molecular sieves regeneration in TSA process: Aliphatic alcohols dewatering-water desorption, Chem. Eng. J. (2015). https://doi.org/10.1016/j.cej.2014.07.108.

[51] J. Wei, Q. Ge, R. Yao, Z. Wen, C. Fang, L. Guo, H. Xu, J. Sun, Directly converting CO2 into a gasoline fuel, Nat. Commun. (2017). https://doi.org/10.1038/ncomms15174.

[52] P. Maksimov, A. Laari, V. Ruuskanen, T. Koiranen, J. Ahola, Gas phase methanol synthesis with Raman spectroscopy for gas composition monitoring, RSC Adv. (2020). https://doi.org/10.1039/d0ra04455e.

[53] J. Schumann, T. Lunkenbein, A. Tarasov, N. Thomas, R. Schlögl, M. Behrens, Synthesis and Characterisation of a Highly Active Cu/ZnO:Al Catalyst, ChemCatChem. (2014). https://doi.org/10.1002/cctc.201402278.

[54] R. Lin, J. Liu, Y. Nan, D.W. Depaoli, L.L. Tavlarides, Kinetics of water vapor adsorption on single-layer molecular sieve 3A: Experiments and modeling, Ind. Eng. Chem. Res. (2014). https://doi.org/10.1021/ie5024645.

[55] W.E. Schiesser, Method of Lines PDE Analysis in Biomedical Science and Engineering, 2016. https://doi.org/10.1002/9781119130499.

[56] W.E. Schiesser, A mathematical modeling approach to infectious diseases: Cross diffusion PDE models for epidemiology, 2018. https://doi.org/10.1142/10954.

[57] A. Vande Wouwer, P. Saucez, C. Vilas, Simulation of ODE/PDE models with MATLAB®, OCTAVE and SCILAB: Scientific and engineering applications, 2014. https://doi.org/10.1007/978-3-319-06790-2.

[58] F. Nestler, A.R. Schütze, M. Ouda, M.J. Hadrich, A. Schaadt, S. Bajohr, T. Kolb, Kinetic modelling of methanol synthesis over commercial catalysts: A critical assessment, Chem. Eng. J. (2020). https://doi.org/10.1016/j.cej.2020.124881.

[59] G.H. Graaf, E.J. Stamhuis, A.A.C.M. Beenackers, Kinetics of low-pressure methanol synthesis, Chem. Eng. Sci. (1988). https://doi.org/10.1016/0009-2509(88)85127-3.

[60] G.H. Graaf, H. Scholtens, E.J. Stamhuis, A.A.C.M. Beenackers, Intra-particle diffusion limitations in low-pressure methanol synthesis, Chem. Eng. Sci. (1990). https://doi.org/10.1016/0009-2509(90)85001-T.

[61] G.H. Graaf, J.G.M. Winkelman, Chemical Equilibria in Methanol Synthesis Including the Water-Gas Shift Reaction: A Critical Reassessment, Ind. Eng. Chem. Res. (2016). https://doi.org/10.1021/acs.iecr.6b00815.

[62] K.M. Vanden Bussche, G.F. Froment, A steady-state kinetic model for methanol synthesis and the water gas shift reaction on a commercial Cu/ZnO/Al2O3 catalyst, J. Catal. (1996). https://doi.org/10.1006/jcat.1996.0156.

[63] N. Park, M.J. Park, Y.J. Lee, K.S. Ha, K.W. Jun, Kinetic modeling of methanol synthesis over commercial catalysts based on three-site adsorption, Fuel Process. Technol. (2014). https://doi.org/10.1016/j.fuproc.2014.03.041.

[64] T.S. Askgaard, J.K. Nørskov, C. V. Ovesen, P. Stoltze, A kinetic model of methanol synthesis, J. Catal. (1995). https://doi.org/10.1006/jcat.1995.1250.

[65] G. Soave, Equilibrium constants from a modified Redlich-Kwong equation of state, Chem. Eng. Sci. (1972). https://doi.org/10.1016/0009-2509(72)80096-4.

[66] L. Pompilio, D. DePaoli, N. Spencer, Evaluation of INL Supplied MOOSE/OSPREY Model: Modeling Water Adsorption on TYper 3A Molecular Sieve, 2014.

[67] M. Schwaab, J.C. Pinto, Optimum reference temperature for reparameterization of the Arrhenius equation. Part 1: Problems involving one kinetic constant, Chem. Eng. Sci. (2007). https://doi.org/10.1016/j.ces.2007.02.020.

[68] T.F. Coleman, Y. Li, An interior trust region approach for nonlinear minimization subject to bounds, SIAM J. Optim. (1996). https://doi.org/10.1137/0806023.

[69] B. Efron, R. Tibshirani, Bootstrap methods for standard errors, confidence intervals, and other measures of statistical accuracy, Stat. Sci. (1986). https://doi.org/10.1214/ss/1177013815.

[70] R.A. Sohn, W. Menke, Application of maximum likelihood and bootstrap methods to nonlinear curve-fit problems in geochemistry, Geochemistry, Geophys. Geosystems. (2002). https://doi.org/10.1029/2001gc000253.

[71] Y. Yu, Y. Wang, K. Lin, N. Hu, X. Zhou, S. Liu, Complete Raman spectral assignment of methanol in the C-H stretching region, J. Phys. Chem. A. (2013). https://doi.org/10.1021/jp400886y.

[72] J.S. Lee, K.H. Lee, S.Y. Lee, Y.G. Kim, A comparative study of methanol synthesis from CO2/H2 and CO/H2 over a Cu/ZnO/Al2O3 catalyst, J. Catal. (1993). https://doi.org/10.1006/jcat.1993.1342.

[73] B. Peng, H. Dou, H. Shi, E.E. Ember, J.A. Lercher, Overcoming Thermodynamic Limitations in Dimethyl Carbonate Synthesis from Methanol and CO2, Catal. Letters. (2018). https://doi.org/10.1007/s10562-018-2402-8.

[74] J. van Kampen, J. Boon, F. van Berkel, J. Vente, M. van Sint Annaland, Steam separation enhanced reactions: Review and outlook, Chem. Eng. J. (2019). https://doi.org/10.1016/j.cej.2019.06.031.

[75] R. Delmelle, J. Terreni, A. Remhof, A. Heel, J. Proost, A. Borgschulte, Evolution of water diffusion in a sorption-enhanced methanation catalyst, Catalysts. (2018). https://doi.org/10.3390/catal8090341.

[76] G. hua Xiu, J.L. Soares, P. Li, A.E. Rodrigues, Simulation of five-step one-bed sorption-enhanced reaction process, AIChE J. (2002). https://doi.org/10.1002/aic.690481210.

[77] T.C. Horng, M. Ajlan, L.L. Lee, K.E. Starling, M. Ajlan, Generalized Multiparameter

Correlation for Nonpolar and Polar Fluid Transport Properties, Ind. Eng. Chem. Res. (1988). https://doi.org/10.1021/ie00076a024.

[78] B. Poling, J. Prausnitz, J. O'Connell, The Properties of Gases and Liquids, 5th ed., McGraw-Hill Companies, Inc, 2001. https://doi.org/DOI: 10.1036/0070116822.

[79] S. Yagi, D. Kunii, N. Wakao, Studies on axial effective thermal conductivities in packed beds, AIChE J. (1960). https://doi.org/10.1002/aic.690060407.

[80] C.H. Li, B.A. Finlayson, Heat transfer in packed beds-a reevaluation, Chem. Eng. Sci. (1977). https://doi.org/10.1016/0009-2509(77)80143-7.

[81] E.N. Fuller, P.D. Schettler, J.C. Giddings, A new method for prediction of binary gas-phase diffusion coefficients, Ind. Eng. Chem. (1966). https://doi.org/10.1021/ie50677a007.

[82] B.J. Lommerts, G.H. Graaf, A.A.C.M. Beenackers, Mathematical modeling of internal mass transport limitations in methanol synthesis, Chem. Eng. Sci. (2000). https://doi.org/10.1016/S0009-2509(00)00194-9.

[83] M.F. Edwards, J.F. Richardson, Gas dispersion in packed beds, Chem. Eng. Sci. (1968). https://doi.org/10.1016/0009-2509(68)87056-3.

[84] B.E. Logan, Environmental Transport Processes: Second Edition, 2012. https://doi.org/10.1002/9781118230107.